

## ESI

# Dielectrics and Possible Ferroelectricity in Diol/Glycerol Covalently Grafted Kaolinites

Zhi-Rong Feng,<sup>a</sup> Bao-Bo Wang,<sup>a</sup> Hao Dong,<sup>a</sup> Shun-Ping Zhao,<sup>c</sup> Yu-Ping Wu,<sup>b</sup> Qiao Qiao,<sup>\*a,b</sup> and Xiao-Ming Ren<sup>\*a,d</sup>

<sup>a</sup> State Key Laboratory of Materials-Oriented Chemical Engineering and College of Chemistry and Molecular Engineering, Nanjing Tech University, Nanjing 211816, P. R. China

<sup>b</sup> School of Energy Science and Engineering, Nanjing Tech University, Nanjing 211816, P. R. China

<sup>c</sup> Anhui Provincial Laboratory of Optoelectronic and Magnetism Functional Materials and School of Chemistry and Chemical Engineering, Anqing Normal University, Anqing 246011, P. R. China

<sup>d</sup> State Key Laboratory of Coordination Chemistry, Nanjing University 210023, P. R. China

Tel.: +86 25 58139476

Email: [qqiao@njtech.edu.cn](mailto:qqiao@njtech.edu.cn) (QQ); [xmren@njtech.edu.cn](mailto:xmren@njtech.edu.cn) (XMR)

## Contents

### Details for crystal structure optimization

**Fig. S1.** SEM images of (a) K and (b) K-DMSO, respectively. (c) PXRD patterns of raw Kaolinite and K-DMSO, respectively, in the  $2\theta$  range of  $5-50^\circ$ .

**Fig. S2.** PXRD patterns of (a) K-PD, (b) K-BD and (c) K-GL in  $2\theta$  ranges of  $5-50^\circ$ , after vigorous stirred in  $H_2O$ , respectively.

**Fig. S3.** (a) The first derivative TG curves of K, K-PD, K-BD and K-GL between 298 and 1073 K, respectively. (b) DSC curves of K between 273 and 553 K.

**Fig. S4.** Plots of  $\text{Tan}(\delta)$ -T at the selected frequency for (a) K-PD, (b) K-BD and (c) K-GL.

**Fig. S5.** Plots of polarization (left) and current density (right) versus electric field of (a) K-PD, (b) K-BD and (c) K-GL after evaporated Au electrode.

**Table S1:** basal plane distance ( $d_{001}$ ) of K-PD, K-BD, K-GL vs. reported literature.

**Table S2:** Mass percentage and theoretical formula of K-PD, K-BD and K-GL.

**Table S3:** Characteristic IR vibration bands and their assignments ( $\text{cm}^{-1}$ ) in K, K-PD, K-BD and K-GL.

### References

### Details for crystal structure optimization

The geometry optimization of crystal structure was performed for K-PD, K-BD and K-GL in the density functional theory (DFT) framework. The Cambridge sequential total energy package (CASTEP) module<sup>1</sup> was employed in the DFT calculation. The total plane-wave pseudopotential method forms the basis of the CASTEP calculations. The exchange-correlation effects were treated within the generalized gradient approximation (GGA) with the Perdew-Burke-Ernzerhof functional.<sup>2</sup> The plane-wave basis set energy cut off was set at 340 eV for K-PD, K-BD and K-GL. The convergence parameters were set as follows: self-consistent field (SCF) tolerance,  $1 \times 10^{-6}$  eV/atom; total energy tolerance  $1 \times 10^{-5}$  eV/atom; maximum force tolerance, 0.03 eV/Å; maximum stress component, 0.05 GPa; and displacement of convergence tolerance, 0.001 Å. All above limits can accurately constrain the simulative process to end at the stable constructions of K-PD, K-BD and K-GL. The other calculation parameters were set at the default values in the CASTEP code. In the geometry optimization process, the unit cell parameters ( $a$ ,  $b$ ,  $\alpha$ ,  $\beta$  and  $\gamma$ ) and the coordinates of all atoms were optimized, while the c-axis length was fixed to the value which was taken from the PXRD measurement. The initial monolayer structure of Kaolinite was taken from the single crystal structure of the raw Kaolinite.<sup>3</sup> Since K-PD, K-BD and K-GL can be expressed in the formula of (K)(PD)<sub>0.87</sub>, (K)(BD)<sub>0.16</sub> and (K)(GL)<sub>0.21</sub>(Table S2), the covalently grafting molecule occupancy was set to be 0.87, 0.16 and 0.21 in the geometry optimization process of K-PD, K-BD and K-GL.

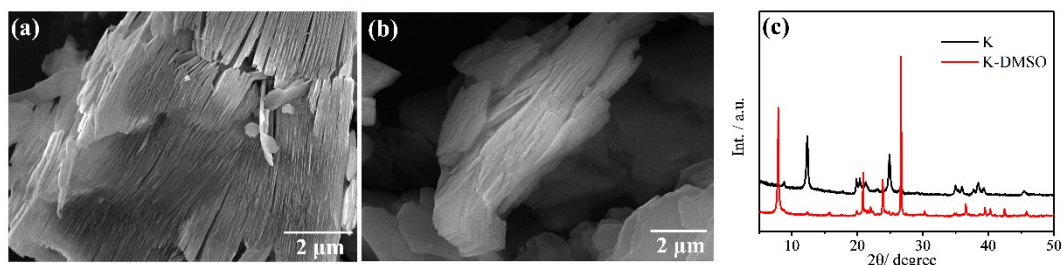


Fig. S1. SEM images of (a) K and (b) K-DMSO, respectively. (c) PXRD patterns of raw Kaolinite and K-DMSO, respectively, in the  $2\theta$  range of 5-50°.

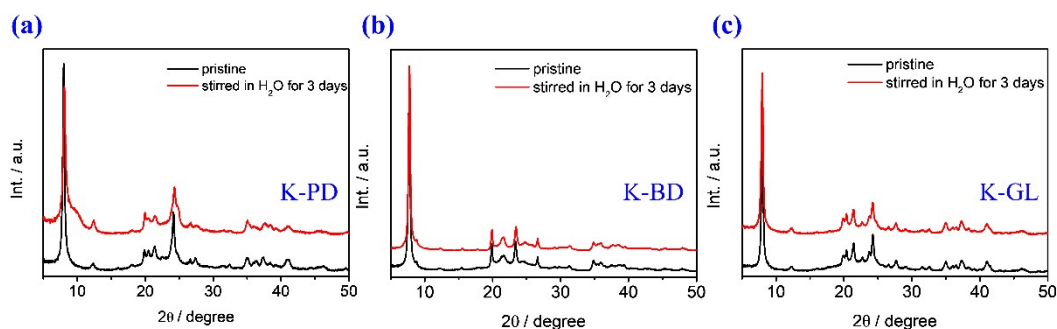


Fig. S2. PXRD patterns of (a) K-PD, (b) K-BD and (c) K-GL in  $2\theta$  ranges of  $5-50^\circ$ , after vigorous stirred in  $H_2O$ , respectively.

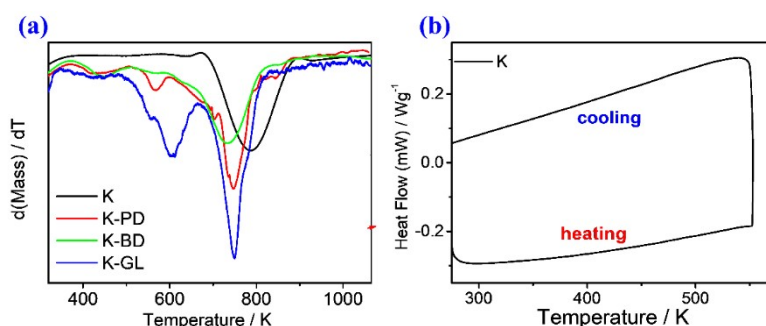


Fig. S3. (a) The first derivative TG curves of K, K-PD, K-BD and K-GL between 298 and 1073 K, respectively. (b) DSC curves of K between 273 and 553 K.

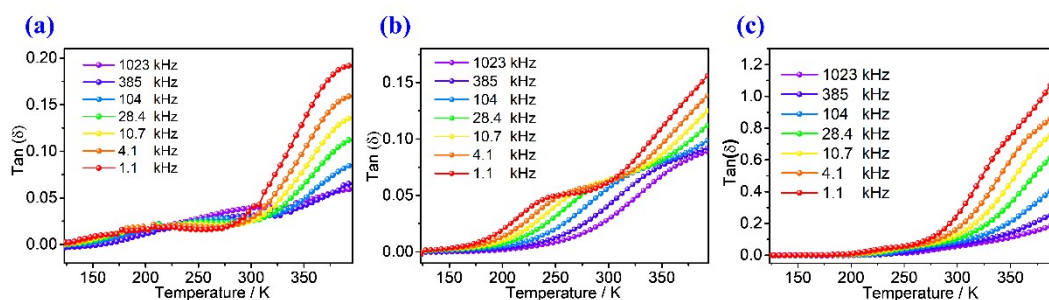


Fig. S4. Plots of  $\text{Tan}(\delta)$ -T at the selected frequency for (a) K-PD, (b) K-BD and (c) K-GL.

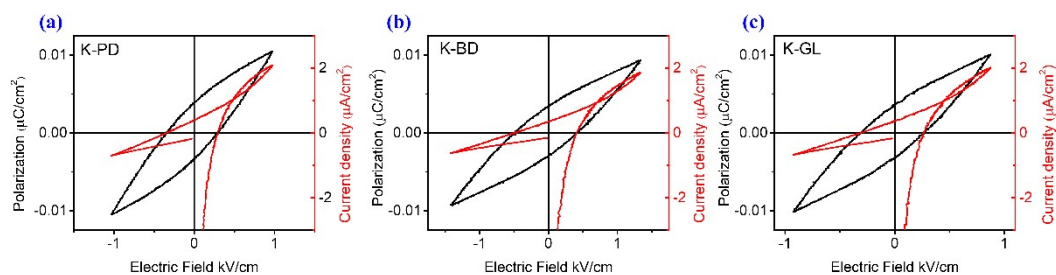


Fig. S5. Plots of polarization (left) and current density (right) versus electric field of (a) K-PD, (b) K-BD and (c) K-GL after evaporated Au electrode.

Table S1: basal plane distance ( $d_{001}$ ) of K-PD, K-BD, K-GL vs. reported literature

Guest molecular	Intercalated compound	$d_{001}(\text{Å})$	$d_{001}(\text{Å})$ (Ref)
1,3-Propanediol	K-PD	11.08	11.13 <sup>4</sup>
1,4-Butanediol	K-BD	11.54	11.61 <sup>5</sup>
Glycerol	K-GL	11.05	11.10 <sup>6</sup>

Table S2: Mass percentage and theoretical formula of K-PD, K-BD and K-GL

	C (mass%) <sup>a</sup>	H (mass%) <sup>a</sup>	N (mass%) <sup>a</sup>	Theoretical formula <sup>b</sup>
K-PD	15.45	4.56	/	(K) (PD) <sub>0.87</sub>
K-BD	2.78	2.2	/	(K) (BD) <sub>0.16</sub>
K-GL	3.59	2.8	/	(K) (GL) <sub>0.21</sub>

<sup>a</sup>Mass percentage tested by Element Analyses, <sup>b</sup> Kaolinite represent  $\text{Al}_2\text{Si}_2\text{O}_5(\text{OH})_4$  abbreviated as K, 1,3-Propanediol, 1,4-Butanediol and Glycerol abbreviated as PD, BD and GL.

Table S3: Characteristic IR vibration bands and assignments ( $\text{cm}^{-1}$ ) in K, K-PD, K-BD and K-GL

K	K-PD	K-BD	K-GL	Assignment
3696, 3650, 3621	3697, 3658, 3622	3698, 3656, 3622	3696, 3659, 3621	$\nu(\text{OH})_{\text{inner \& inner surface}}$
1116, 1066, 1033	1117, 1065, 1030	1114, 1065, 1029	1116, 1065, 1031	$\nu_{\text{as}}(\text{Si-O})$
696, 468, 428	693, 472, 431	695, 471, 432	698, 472, 430	$\delta(\text{Si-O})$
914	909	911	912	$\beta(\text{Al-OH})$
/	3449	3450	3448	$\nu_{\text{as}}(\text{O-H})$ of $\text{H}_2\text{O}$
/	1632	1632	1635	$\beta(\text{O-H})$ of $\text{H}_2\text{O}$
/	2974	2973	2975	$\nu_{\text{as}}(\text{CH}_2)$
/	2896	2897	2899	$\nu_{\text{s}}(\text{CH}_2)$

## References

- 1 M. D. Segall, P. J. D. Lindan, M. J. Probert, C. J. Pickard, P. J. Hasnip, S. J. Clark and M. C. Payne, *J. Phys-Condens. Mat.*, 2002, **14**, 2717.
- 2 J. P. Perdew, K. Burke and M. Ernzerhof, *Phys. Rev. Lett.*, 1996, **77**, 3865.
- 3 D. L. Bish, *Clay. Clay. Miner.*, 1993, **41**, 738.
- 4 M. Janek, K. Emmerich, S. Heissler and R. Nüesch, *Chem. Mater.*, 2007, **19**, 684–693.
- 5 J. J. Tunney and C. Detellier, *Chem. Mater.*, 1993, **5**, 747–748.
- 6 J. Murakami, T. Itagaki and K. Kuroda, *Solid State Ionics*, 2004, **172**, 279–282.



# Graphical Abstracts

